Synchronization of great subduction megathrust earthquakes: Insights from scale model analysis

Matthias Rosenau[1], Illia Horenko[2], Fabio Corbi[3,4], Michael Rudolf[1], Ralf Kornhuber[5], Onno Oncken[1]

[1]Department of Geomaterials, Helmholtz Centre Potsdam, GFZ German Research Centre for Geosciences, Potsdam, Germany

[2]Department of Mathematics and Computer Science, Università della Svizzera Italiana, Lugano, Switzerland

[3]Department of Science, Roma Tre University, Rome, Italy

[4]Géosciences Montpellier, CNRS, University of Montpellier, Montpellier, France

[5] Department of Mathematics and Computer Science, Free University Berlin, Berlin, Germany

Pre-print

Please cite as:

Rosenau, M., Horenko, I., Corbi, F., Rudolf, M., Kornhuber, R. and Oncken, O. (2017): Synchronization of great subduction megathrust earthquakes: Insights from scale model analysis. SFB 1114 Preprint in EarthArXiv. pp. 1-35. https://dx.doi.org/10.17605/OSF.IO/PQ2U3

Abstract

The size of great subduction megathrust earthquakes is controlled mainly by the number of adjacent asperities failing synchronously and the resulting rupture length. Here we investigate experimentally the long-term recurrence behavior of a pair of asperities coupled by quasi-static stress transfer over hundreds of seismic cycles. We statistically analyze long (c. 500 ka) time-series of M8-9 analogue earthquakes simulated using a seismotectonic scale model approach with two aims: First, to constrain probabilistic measures (frequency-size distribution, variability) useful for hazard assessment and, second, to relate them with geometric observables (coseismic slip pattern, locking pattern). We find that the number of synchronized failures (double events) relative to the number of individual failures (solo events) as well as the coefficient of variation of recurrence intervals scale with the logarithm of stress coupling between the asperities. Tighter packed asperities tend to recur more periodically while more distant asperities show clustering. The probability of synchronized failures is controlled to first order by geometrical relations (size and distance of asperities). The effects of rheological properties are evident but it remains to be explored to which extent they vary in nature and how sensitive the system is to those.

1. Introduction

Giant magnitude 9 earthquakes unzip up to 1000 km long segments of active plate margins. Such long ruptures include failure of several asperities. Pre-requisites to fail synchronously (or sequentially in short succession, i.e. within seconds) are a homogeneous high stress level along the margin (i.e. in a late interseismic stage in different segments of the megathrust) and a trigger for nucelation which might be very small depending on the state of synchronization. Ruff (1996) introduced the idea of synchronization of the seismic cycle "clocks" in subduction zones by static stress transfer leading to giant earthquakes. He developed and analyzed a simple mechanical model consisting of two frictional spring-sliders coupled by a spring as an analogon of a segmented subduction zone with segments interacting by means of stress coupling (Fig. 1). He hypothesized that while individual recurrence times may initially be different (controlled by the individual frictional strength and spring stiffness) stress coupling may introduce variability and cause synchronization over multiple seismic cycles..

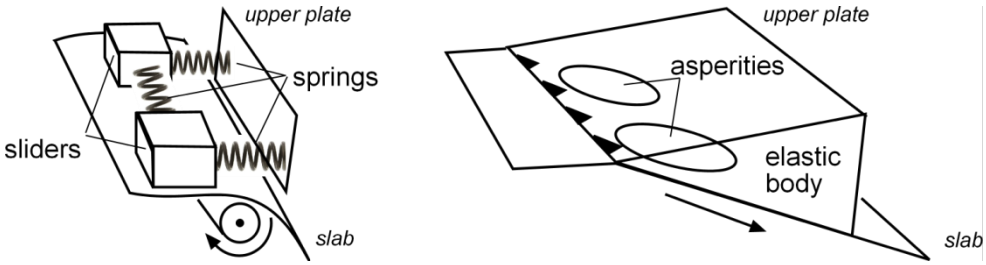

Figure 1: The concept of stress coupling and synchronization in subduction zones by means of coupled spring sliders as depicted by Ruff (1996) and the modern transformation of the idea by means of asperities coupled by elastic stress transfer in an elastic medium.

In a modern view Ruff's (1996) idea is based on clock advances triggered by static (Coulomb) stress transfer between asperities embedded in an elastic medium (Figure 1).

The first to model such a system realistically were Kaneko et al. (2010). They came up with a fully dynamic simulation of a pair of coseismically weakening asperities separated by a coseismically strengthening barrier. This simulation demonstrated the role of the size and rheology of the barrier in controlling rupture propagation across it. Because of the computational costs of such numerical models, the lengths of the simulated earthquakes where rather limited to few tens of cycles.

Here we realize those models by means of seismotectonic scale modelling (Rosenau et al., 2017a) which allows a realistic simulation of comparatively long analogue earthquake sequences with up to 500 individual events at a rather low experiment and time cost compared to numerical simulation. We simulate a subduction zone forearc wedge in an archetypical setup with two seismogenic asperities characterized by velocity-weakening and unstable stick-slip frictional behavior. The asperities are surrounded by velocity-strengthening material displaying stable creep and acting as a barrier to seismic slip. Stress coupling by means of static Coulomb stress transfer is realistically implemented by the elastic wedge and quantified using elastic dislocation modelling. While frictional and elastic properties are kept constant we vary the relative position of the two asperities along strike and across strike allowing us to explore the effects of variable stress coupling and strength contrasts between the two asperities.

Our study complements and extends recent analogue models by Corbi et al. (2017) who tested the geometric aspects of Kaneko et al. (2010) simulation using a seismotectonic scale model similar to the one we use. They were able to verify experimentally the major role of the geometric relation between the asperities in synchronization. While they were able to reproduce both the numerical results by Kaneko et al. (2010) as well as the natural observations from Japan, the significance of frictional properties remained unexplored by Corbi et al. (2017).

Here we complement these studies first by providing an analogue model with a different set of frictional properties compared to Corbi et al. (2017) to allow testing their significance more specifically. Second, we introduce a strength contrast between the two asperities, a factor which has not been tested experimentally or numerically so far. Third, we generated about 10 times longer analogue sequences (up to 0.5 Million years long including several hundreds of M8-M9 events) allowing a more rigorous statistical analysis and more reliable tests for statistical significance.

2. Modelling and analysis methods

2.1 Seismotectonic scale modelling of a subduction megathrust setting

2.1.2 Experimental setup and scaling

Seismotectonic scale modelling is a cost-effective method to simulate long earthquake sequences in a fully three-dimensional, dynamic and spatiotemporally quasi-continuous framework (e.g. Rosenau et al. 2009, 2017, Corbi et al., 2013, 2017, Caniven et al. 2015, 2017). Here we recall the basics of the approach and report modifications specific to the present study.

The experimental setup used in this study is a development from an earlier quasi-two-dimensional setup used for seismotectonic scale modelling by Rosenau et al. (2009, 2010) where the method has been explained in detail. The setup used in the current study is six-times wider and therefore truly 3D and allows simulating along-strike rupturing of analogue earthquakes. The experimental device consists of a glass-sided box (100 cm across strike, 60 cm along strike and 50 cm deep) with a 15° dipping basal conveyer plate on top of which a compressive wedge (subduction forearc model) is set up at appropriate scale and compressed against a rigid and fixed backwall (Figure 2a).

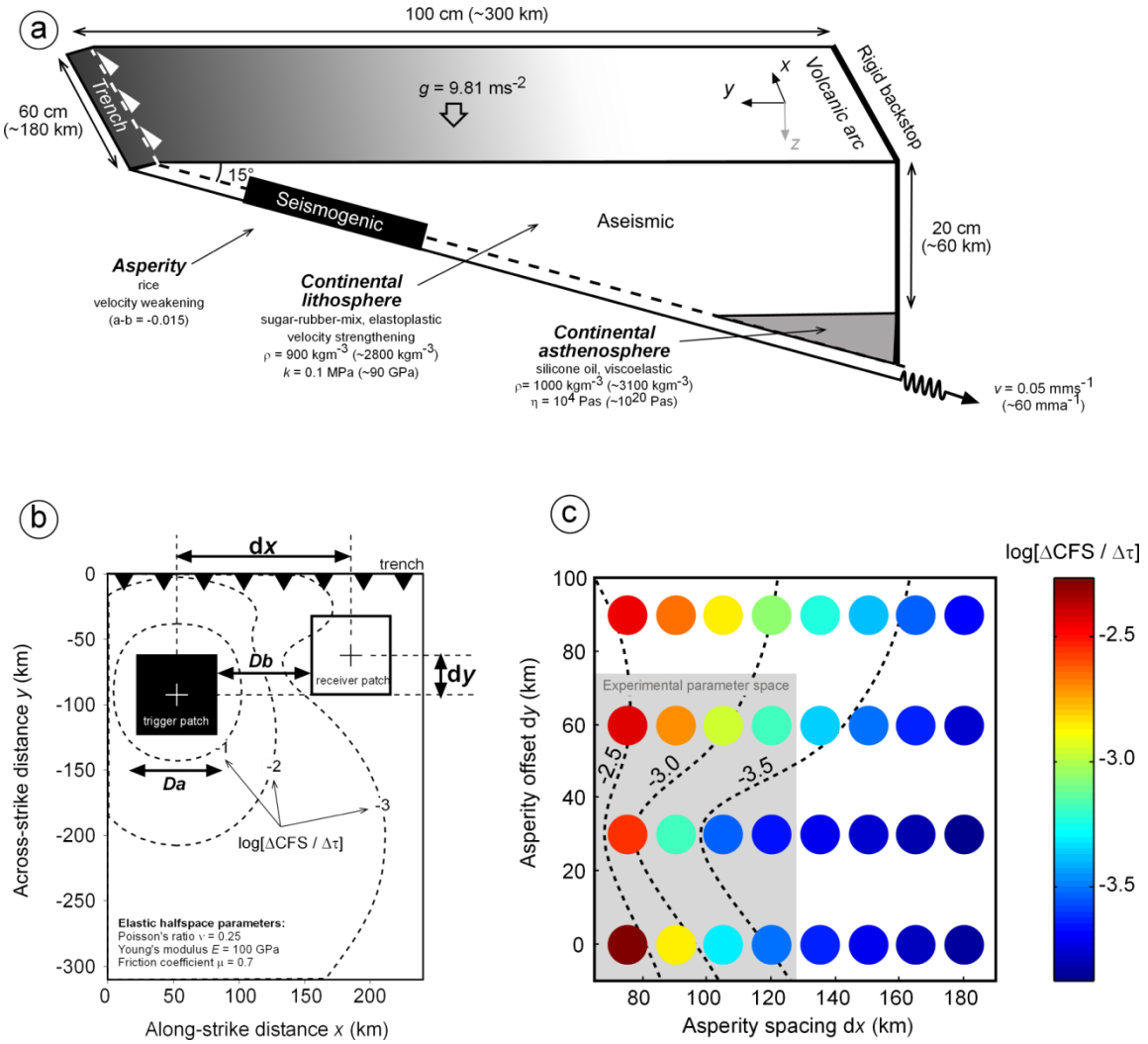

Figure 2: Seismotectonic scale model setup: (a) 3D view of analogue model setup (cross-section corresponds to x = 50 km in (b)); (b) Map-view (surface projection) of megathrust setup with calculated Coulomb stress changes dCFS (normalized to stress drop dTau on trigger asperity) indicated (note the logarithmic fall-off with distance from the trigger asperity). Da and Db refer to the parameters used by Corbi et al. (2017). (c) Parameter space: Asperity spacing (dx) and offset (dy) and corresponding stress coupling log(dCFS/dTau) in color and isolines. Grey shaded area corresponds to the subspace realized experimentally. Size of the asperities has not been changed in this study.

Dynamic similarity of the laboratory scale model with the natural prototype requires the ratios of forces, which are expressed as dimensionless numbers, to be the same as in nature. We use the following set of dimensionless numbers to ensure similarity with respect to strength σ, gravity *G*, and inertia *I*:

1. The ratio τ between gravitation and strength (either elastic, frictional or viscous) is

$$\tau = \rho \cdot l \cdot g / \sigma \quad (1)$$

where ρ is the rock density, l is a characteristic length, g is the gravitational acceleration, and σ is the elastic, frictional or viscous strength.

2. The *Froude Number Fr* relates gravitation and inertia and is

$$Fr = v \cdot (g \cdot l)^{-0.5} \quad (2)$$

where v is a characteristic velocity.

3. The *Cauchy Number Ca* relates inertia and elasticity and is

$$Ca = \rho v^2 / k \quad (3)$$

where k is the bulk modulus.

By keeping these dimensionless numbers the same in an experiment executed in the earth's gravity field as in nature, the following scaling relationships are derived from equations (1) to (3):

$$\tau^* = \tau \rightarrow (\sigma^*/\sigma) = (\rho^*/\rho) \cdot (l^*/l) \quad (4)$$

$$Fr^* = Fr \rightarrow (t^*/t) = (l^*/l)^{0.5} \quad (5)$$

$$Ca^* = Ca \rightarrow (k^*/k) = (\rho^*/\rho) \cdot (l^*/l)^2 \cdot (t/t^*)^2 \quad (6)$$

where "*" marks the model numbers and values. The ratios between model and natural prototype values are known as the scaling factors [Hubbert, 1937].

These scaling relationships dictate the experimental conditions and material properties (Tab. 1) for a given length scale and material density. The model materials used here are three times less dense and designed at a length scale $(l^*/l) = 3.3 \cdot 10^{-6}$ such that 1 cm in the scale model corresponds to 3 km in nature. According to equations (4) – (6) it follows that the scale model

has to be weaker than the natural prototype by a factor (σ^*/σ) = $1.1 \cdot 10^{-6}$ and should deform ~ 500 times slower during analogue earthquakes in order to properly scale the body forces. The corresponding coseismic time scale is (t^*/t) = $1.8 \cdot 10^{-3}$ (i.e. 0.1 second in the lab corresponds to about 50 seconds in nature). Because this dynamic time scale would result in unsuitable long recurrence intervals of analogue earthquakes in the laboratory and because inertial forces can be neglected during the quasi-static inter-event time we scale the interseismic periods with a factor derived from the ratio of the viscosity scale and the stress scale ($1.3 \cdot 10^{-10}$; 1 second in the lab scales to ~ 250 years).

Note that scale models represent strong simplifications of the natural prototype and their application is always limited. See Rosenau et al. (2017) for a review of the seismotectonic scale modelling approach.

2.1.2 Scale model configuration and material properties

The generalized subduction zone model presented here is analogous to a 300-km-wide and 180 km long forearc section from the trench to the volcanic arc (Figure 2a). The scale model is made up of a granular wedge of elastic-frictional plastic (elastoplastic) mixtures of EPDM (ethylene propylene diene monomer) rubber pellets with refined sugar and flavored rice representing the brittle forearc lithosphere. The wedge overlies silicone oil representing the viscoelastic asthenosphere. We generalize the natural subduction geometry by considering a planar, 15°-dipping megathrust between an upper plate made up of ~ 60-km-thick lithosphere and ~ 20-km thick asthenosphere below the arc and an oceanic plate. The latter is represented by a conveyer plate pulled constantly via a spring-loaded thrust pad at 50 μm/s simulating plate convergence at a long-term rate of about 60 mm/a in nature.

The model megathrust is defined by a few millimeters wide shear zone which forms at the base of the wedge ("subduction channel", *Shreve and Cloos* [1986]). It is characterized by rate- and state-dependent frictional behavior similar to nature [*Scholz*, 1998]. In particular, it

includes two patches (20 cm x 20 cm ~ 60 km x 60 km) displaying stick-slip deformation and mimicking a pair of seismogenic asperities separated by an aseismic barrier. The friction rate-parameter *a-b* within the asperities, made up of rice, is ~ -0.015. The barrier separating the two asperities as well as up- and downdip regions of the asperities are characterized by aseismic slip or stable sliding (creep) controlled by the velocity strengthening behavior (*a-b* ~ +0.015) of frictional slip in sugar. Material properties of this seismotectonic scale model have been documented in detail in Rosenau et al. [2009, 2017] and Rudolf et al. (2016) and are reported in Table 1.

The two asperities have an along subduction zone strike center-to-center distance (hereafter called spacing) dx and are a relative shift across subduction zone strike (hereafter called offset) dy (Figure 2b). This configuration allows exploring the effects of stress coupling (as defined below in section 2.2.2) as well as strength contrast. We define the latter as the shear strength of the weaker (shallower) asperity 2 relative to the stronger (deeper) asperity 1:

Strength contrast = Tau2/Tau1 (7)

Strength contrast therefore ranges theoretically from close to 0 to 1. Note the somewhat counter-intuitive effect that low strength contrasts are reflected by Tau2/Tau1 values. In total 12 configurations have been realized in which we vary the strength contrast from 0.6 to 1.0 and the stress coupling from a few ppm to percent (Fig. 2c). The experimental runs took place under normal gravity conditions and in a dry room climate (22 – 23°C, 30 – 40 % humidity).

	Parameters:				**Similarity:**						
	Quantity	Symbol	Dimension {M,L,T}	Unit	Quantitiy	Model		Nature		Dimensionless number	Scaling factor
Model kinematics	Length	l	L	[m]	coseismic slip	29 ± 12	µm	8.8 ± 3.6	m	$Fr = v'/[gl]^{-0.5}$	$3.3 \cdot 10^{-6}$
	Velocity (interseismic)	v	L/T	[m/s]	plate velocity	50	µm/s	60	mm/a		$2.6 \cdot 10^{4}$
	Velocity (coseismic)	v'	L/T	[m/s]	rupture velocity	> 3	m/s	> 2	km/s	$Ca = \rho v'^2/k$	$1.8 \cdot 10^{-3}$
	Graviational acceleration	g	L/T²	[m/s²]		9.81	m/s²	9.81	m/s²	g/a'	1
	Coseismic slip acceleration	a'	L/T²	[m/s²]		0.6	m/s²	0.6	m/s²	g/a'	1
Material properties	Friction coefficient	µ			interseismic	0.7		0.7		φ	1
	Friction rate parameter	a-b			strengthening/weakening	+/- 0.015		+/- 0.015		a-b	1
	Cohesion	C	M/LT²	[Pa]	lithosphere	10	Pa	9	MPa		$1.1 \cdot 10^{-6}$
	Bulk modulus	k	M/LT²	[Pa]	lithosphere	0.1	MPa	90	GPa		$1.1 \cdot 10^{-6}$
	Viscosity	η	M/LT	[Pas]	asthenosphere	10^4	Pas	$7 \cdot 10^{19}$	Pas		$1.4 \cdot 10^{-16}$
	Density	ρ	M/L³	[kg/m³]	lithosphere / asthenosphere	900/1000	kg/m³	2800/3100	kg/m³		$3.3 \cdot 10^{-1}$
Forces	Gravitation	$G = \rho V g$	ML/T²	[N]							$1.2 \cdot 10^{-17}$
	Inertia	$I = \rho V a$	ML/T²	[N]							$1.2 \cdot 10^{-17}$
Energy	Seismic moment	$M_0 = kDA$	ML²/T²	[Nm]	seismic moment	3 ± 2	Nm	$7 \cdot 10^{22} \pm 5 \cdot 10^{22}$	Nm		$4 \cdot 10^{-23}$

Table 1: Analogue model parameters, scaling relations and material properties

2.1.3 Experimental Monitoring and Strain Analysis

For strain analysis of the evolving model wedges we use an optical image acquisition and correlation system (particle image velocimetry, PIV StrainMaster by LaVision, Germany, see *Adam et al.* [2005], *Rosenau et al.* [2009, 2010, 2017] for applications in analogue tectonic and earthquake simulation).

During an experiment, the locations of particles on the model surface (i.e. within the *x*-*y*-plane of the model, Fig. 2) are recorded by sequential 11 Mpx-digital images of a 14-bit monochrome charge-coupled device (CCD) camera acquired at a frequency of 10 Hz. The *x*-*y*-displacement vector field between successive images is then determined by cross-correlation of textural differences (i.e. gray values) formed by groups of particles using a Fast Fourier Transform algorithm. The spatial resolution of the final displacement vector grid is ~

3 mm or about 1 km in nature. For each grid-cell, an average *x*-*z*-displacement vector is determined at micrometer precision (~ decimeter scale in nature). This allows for observing episodic surface deformation events corresponding to earthquakes of moment magnitude M_w >8. Analogue earthquakes are characterized by episodic, usually more than one order-of-magnitude increased strain rates and a change in polarity of the wedge deformation from "landward" motion (in negative y-direction) and compaction during the interseismic stage to "seaward" motion and extension during the coseismic stage (Figure 3 a, b). Earthquakes typically occur within a 0.1-second time interval, i.e. are captured by a solo image.

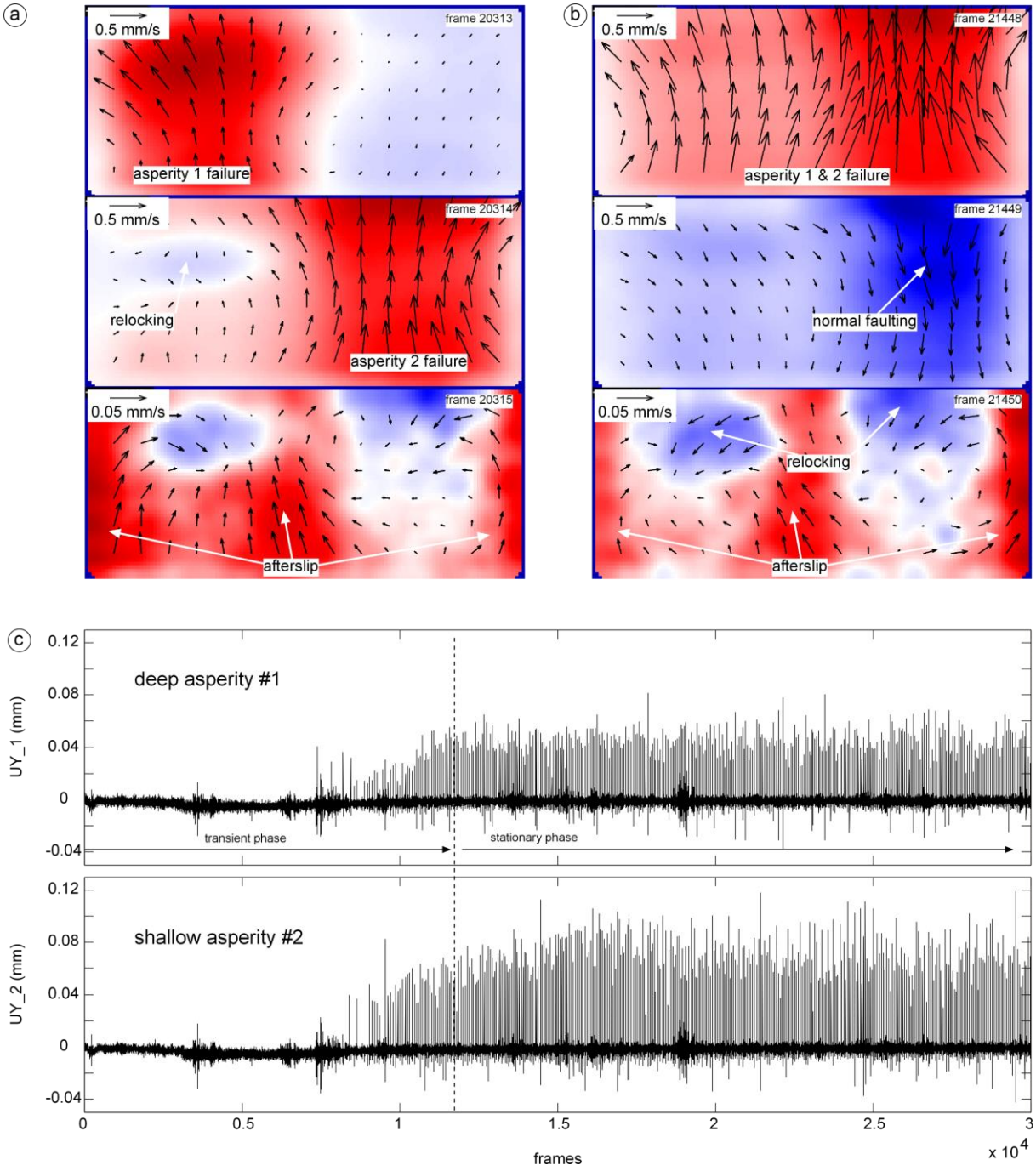

Figure 3: Example of surface deformation pattern on top of the asperities (trench is north): (a) sequence of a cluster of two solo events followed by afterslip and relocking (each velocity field corresponds to 0.1 second experimental time). (b) sequence of a double event followed by a normal event, relocking and afterslip. Note the different vector scale for coseismic (upper, middle panel) and postseismic phases. Colors are scaled to the maximum velocity in each panel (red = surface displacement towards trench, white = 0, blue = away from the trench). (c) time-series of surface deformation towards the trench (UY) averaged over the surface projected area of asperity 1 and asperity 2 used for further analysis. Note the asymmetry in displacements above shallow and deep asperity which is related to the free-surface effect.

2.2 Elastic dislocation modelling

We use elastic dislocation modelling following Okada (1992) and Okada (1985) for coseismic slip inversion and Coulomb stress transfer calculation employing the Matlab-based software package "Coulomb" by Toda et al. (2011, Coulomb 3.3 Graphic-rich deformation and stress-change software for earthquake, tectonic, and volcano research and teaching—user guide: U.S. Geological Survey Open-File Report 2011–1060, 63 p., available at http://pubs.usgs.gov/of/2011/1060). The model setup for elastic modelling uses the scaled values of geometric and mechanical parameters given by the analogue model.

2.2.1 Slip inversion

Surface deformation during analogue earthquakes as captured by PIV is converted into coseismic slip along the megathrust using inversion factors derived by forward elastic dislocation modelling. Accordingly we find the factors relating horizontal surface deformation UY directly above the dislocation at depth to slip S along it to range between 0.2 and 0.5 depending non-linearly on the depth of dislocation (Figure A1). Shallow dislocations show larger factors, i.e. are less attenuated. We do not aim at a formal inversion or distributed slip modelling. Instead we consider here mean coseismic surface displacement over the projected surface area of the asperity to be a valuable proxy for mean coseismic slip over the asperity at depth.

2.2.2 Stress coupling

For quantifying the interaction by means of stress coupling between the asperities we follow the principles of static Coulomb stress transfer (CFS) modelling as established by King et al. (1994) Toda and Stein (2002) and Lin and Stein (2004).

The model setup for CFS modelling is such that we impose thrust slip on one asperity (trigger asperity) and average the predicted CFS increase (dCFS) for thrust faulting on the receiver

asperity (Fig. 2a). We then define a parameter called stress coupling as the CFS increase averaged over the receiver asperity normalized by the stress drop on the trigger asperity:

$$\text{Stress coupling} = dCFS/dTau. \quad (8)$$

In the present setup stress coupling is in the order of less than a ppm up to one percent similar to nature. Stress coupling falls off exponentially with distance and varies non-linearly across-strike of the megathrust as a function of asperity spacing (dx) and offset (dy, Fig. A2).

2.3 Numerical analysis of surface deformation time series

Experimental time-series of surface deformation consist of typically a sequence of 30.000 images and corresponding incremental vector fields. To detect analogue earthquakes from such a big data set we usually rely on computational algorithms sensitive to accelerations validated by visual inspection. However, because of experimental noise such a kinematic approach based on thresholding velocity usually has a high detection limit. Instead of thresholding velocities to detect earthquakes stages we here employ a numerical time-series analysis technique developed in computational statistics. This allows us to detect events which can be below the detection threshold of classical kinematic approaches.

As input we use the surface deformation time-series of mean across-strike velocities UY_1(t) and UY_2(t) in the surface projection area of the two asperities (Figure 3c). Those data typically show a transient phase withithout much activity in the beginning which reflects stress buildup and reorganization within the analogue model (Figure 3c). After about 5.000-10.000 increments (500-1000 seconds) surface accelerations reflecting analogue earthquakes start to occur with increasing size and frequency and quickly reach a quasi-stationary state. We use observations from this quasi-stationary state for further analysis.

To analyze the obtained experimental time series, we deploy a nonparametric time series analysis methodology called Finite-Element-Method with Bounded Variation of model parameters (FEM-BV) (Horenko 2009, Horenko 2010, Metzner et. al. 2012). Although it is computationally more expensive then the common methods, FEM-BV has several important conceptual advantages that were recently illustrated for various time series analysis applications in geosciences (Vercauteren et. al. 2015, Risbey et. al 2015, Franzke et. al. 2015, Kaiser et. al. 2015, O'Kane et. al. 2016). This nonparametric method is automatized, does not rely on any tunable user-defined parameters (like thresholds values for the event identification) and allows to go beyond strong parametric assumptions (like linearity, Gauss or Poisson distribution assumptions for observed densities, stationarity or Markovianity) – assumptions that are a constitutive part of the more common statistical time series analysis approaches like multilinear regression, Hidden Markov Models or clustering methods (e.g. Shearer and Stark, 2012). Going beyond these assumptions is especially important since analyzed data exhibits a strong regime-transition behavior, is non-stationary, non-Markovian and non-Gaussian in the regimes. Moreover, defining ad hoc threshold values for the events could potentially introduce a user-defined bias. We refer to Metzner et. al (2012) for mathematical/statistical details of the FEM-BV methodology – as well as for its computational comparison with more common time series analysis methodologies.

2.4 Statistical analysis of analogue earthquake sequences

Based on the long sequences of analogue earthquakes we explore the recurrence behavior and its intrinsic variability by means of univariate and bivariate statistics.

A simple measure of probability, used by earlier studies as well, is the relative number of events of a given character (e.g. solo events, double/synchronized events). To get further insight into the statistics however, the present studies allows producing probability distribution functions (pdf) of distinct event parameters. We here use the pdf of moment

magnitudes (Figure 4a and A3) to characterize the "Gutenberg-Richter" frequency-size relationship. And we use the pdf of the recurrence interval time (Figure 4c and A3) to differentiate between periodic and aperiodic (e.g. clustered) occurrence of events.

Moreover, we quantify variability of the seismic moment (M0) and recurrence time (Trec) by calculating the associated coefficients of variation:

$$CV = \text{standard deviation} / \text{mean}. \quad (9)$$

CV serves as a first-order proxy for recurrence behavior: a CV of 1 characterizes a random behavior while CV<1 suggests characteristic or periodic recurrence. A CV>1 is characteristic of clustering (e.g. Kuehn et al., 2008, Rosenau and Oncken, 2009).

3 Experimental observations and interpretations

3.1 Seismic performance of the scale model

A typical earthquake catalogue simulated by our scale model consist of up to 500 events of moment magnitude 8-9 which occur over a time-period of about 500 ka (Fig. 4a). M8 events usually involve only one asperity while a synchronous failure of both asperities usually results in the M9 events. Analogue earthquakes are always followed by afterslip lasting for not more than one frame (0.1 s) surrounding the asperities (Figure 3 a, b). Generally the shallow asperity generates more surface displacement than the deep one: This is related to static effects as predicted by elastic dislocation modelling (Figure A1). The picture inverts when the correction for depth of dislocation is applied. Then, deeper asperities show larger slip. This is consistent with higher loads causing higher frictional strength at greater depth as predicted by Mohr-Coulomb theory. As a consequence, the deeper asperities are mechanically stronger and able to accumulate more slip deficit in the interseismic period compared to the shallow asperities.

313 We refer to slip events which occur on both asperities within one time frame (0.1 s) as double
314 or synchronized events. If the second event occurs independently within the next frame, we
315 refer to it as an aftershock or a clustered event. A minority of aftershocks are actually
316 relatively small normal faulting events. We interpret those as a result of dynamic overshoot
317 during the preceding thrust event. Normal events occur almost exclusively in the shallow
318 asperity. We include those rare normal events in our analysis since they represent an integral
319 part of the long-term slip budget. Accordingly, they show up with a negative seismic moment
320 in Figure 4a.
321

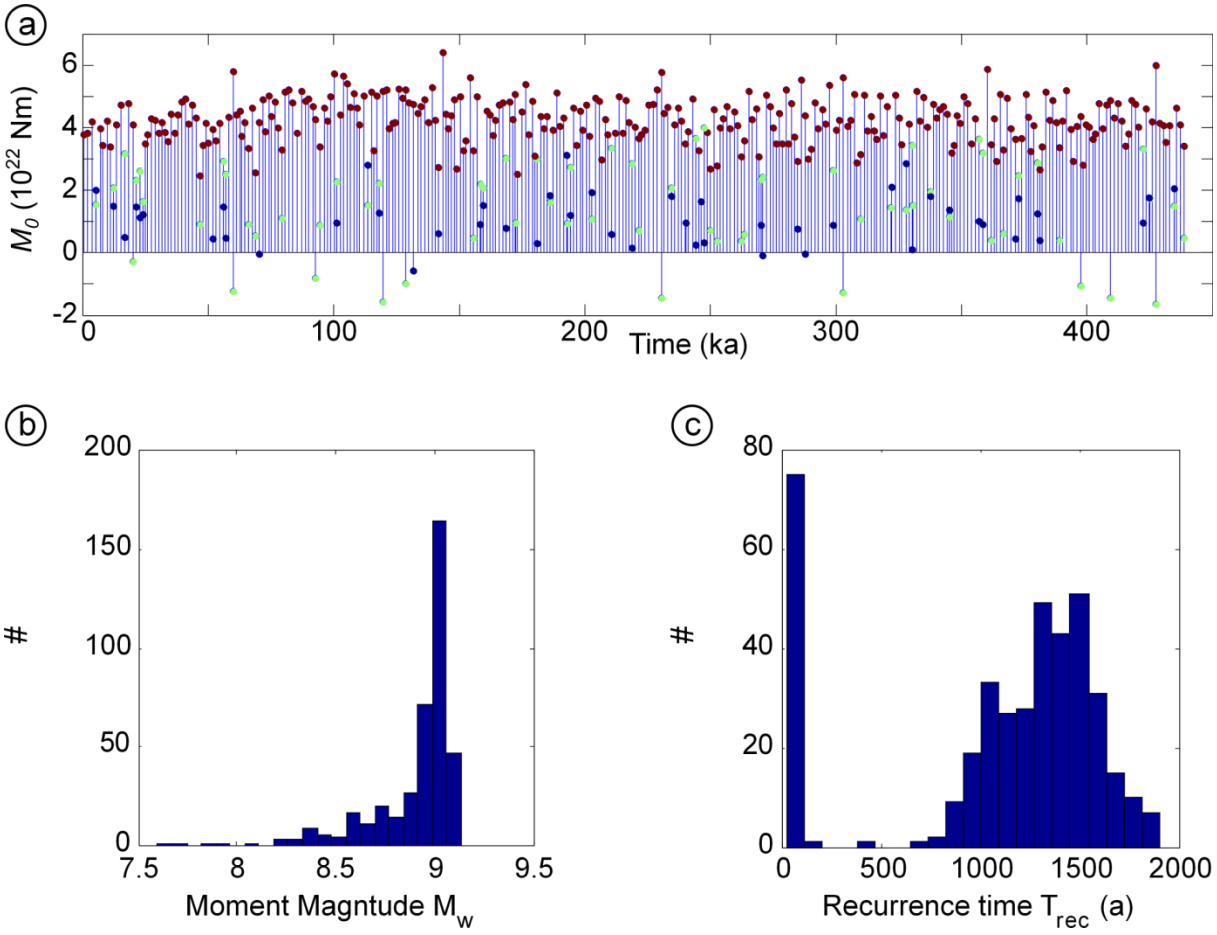

322

323 ***Figure 4****: Example of an earthquake sequence simulated using seismotectonic scale modelling and*
324 *derived by the numerical FEM-BV approach (all parameters scaled to nature): (a) event catalogue:*
325 *(b) pdf of moment magnitude Mw, (c) pdf of recurrence time Trec. See appendix figure A3 for pdfs of*
326 *all experiments.*

327 When analyzing synchronous (double) events, clustered (solo) events and normal events
328 (overshoots) as a function of stress coupling dCFS/dTau and strength contrast Tau2/Tau1 a
329 clear picture emerges (Figure 5). Accordingly, a synchronous double events increase in
330 number from 20 to 80 % as stress coupling increases by two orders of magnitude (from less
331 than a ppm up to a percent). At the same time, clustered events decrease. This simply reflects
332 a higher degree of synchronization in strongly coupled systems. Overshoots show no clear
333 correlation with stress coupling but a negative correlation with strength contrast (Figure 5).
334 This is consistent with overshoots occurring preferentially in shallow regions of the wedge.

Both synchronous double and clustered solo events show no correlation with strength contrast. An apparent increase of the range of proportion of those events with stress contrast reflects the systematically wider range in stress coupling realized for lower strength contrasts.

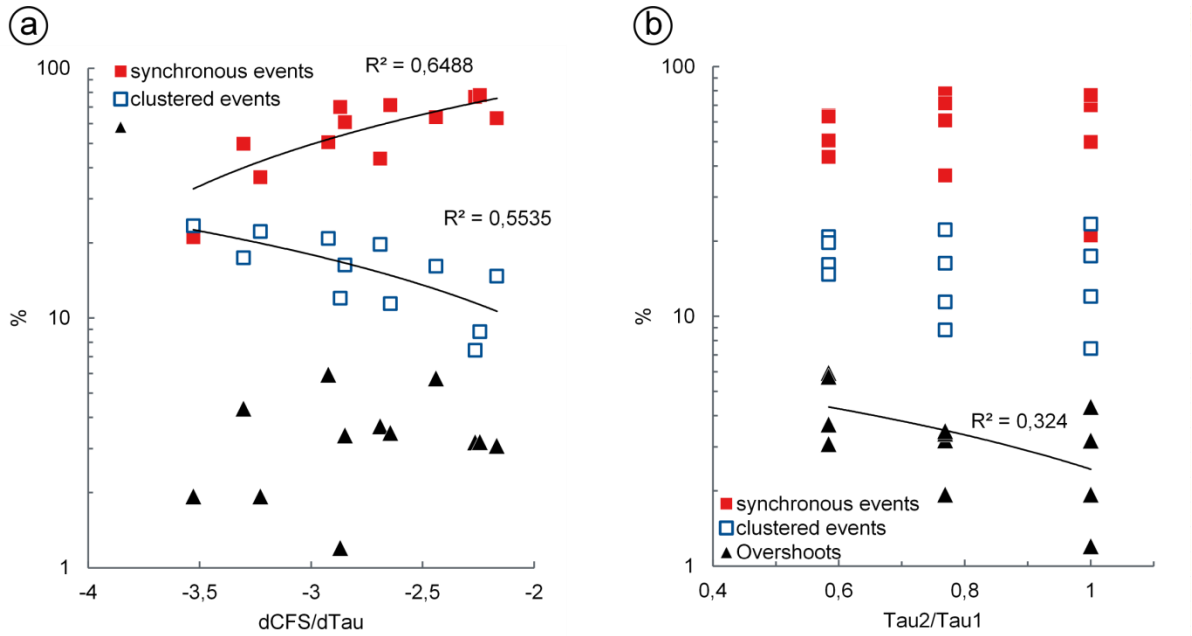

***Figure 5**: Percentage of different types of events versus stress coupling (a) and strength contrast (b).*

3.2 Frequency-size distributions

Frequency-size distributions of simulated earthquakes share similar shapes. The pdfs of moment magnitude are generally skewed negatively (towards the left) and very peaked as exemplified in Figure 4b. The PDFs of recurrence times are generally bimodal characterized by a peak at short periods (0.1 sec or 25 years) and a quasi-normally distributed bump around the mean recurrence time as exemplified in figure 4c.

Plotting mean recurrence times and mean seismic moments and their variability in terms of CV into the parameter space (Figure 6) shows the following: Mean recurrence time and seismic moment both increase with an increase in stress coupling. At the same time their CVs

decrease. R^2-values for these correlations range between 0.3 and 0.6 (Table A1 in appendix) and the trends considered significant.

We interpret this correlation of M_0 and T_{rec} with stress coupling as reflecting a dynamic interaction causing higher slip in case of more strongly coupled asperities. Larger slip consistently lengthens the interseismic period resulting in longer recurrence times. The increase in size seems also to have a positive effect on the periodicity with larger stress drops regulating the earthquake cycle thus decreasing the CV to 0.5.

A weak positive correlation exist between T_{rec} and strength contrast ($R^2 = 0.25$). Accordingly, earthquake frequency increases as the weak asperity becomes weaker. We interpret this as being a behavior predicted by Ruff (1996) where the weaker asperity, which has intrinsically the shorter recurrence time, causes clock advance of the stronger asperity, which has intrinsically longer recurrence times. A correlation between M_0 as well as the associated CVs with strength contrast have not been observed to be statistically significant ($R^2 < 0.05$).

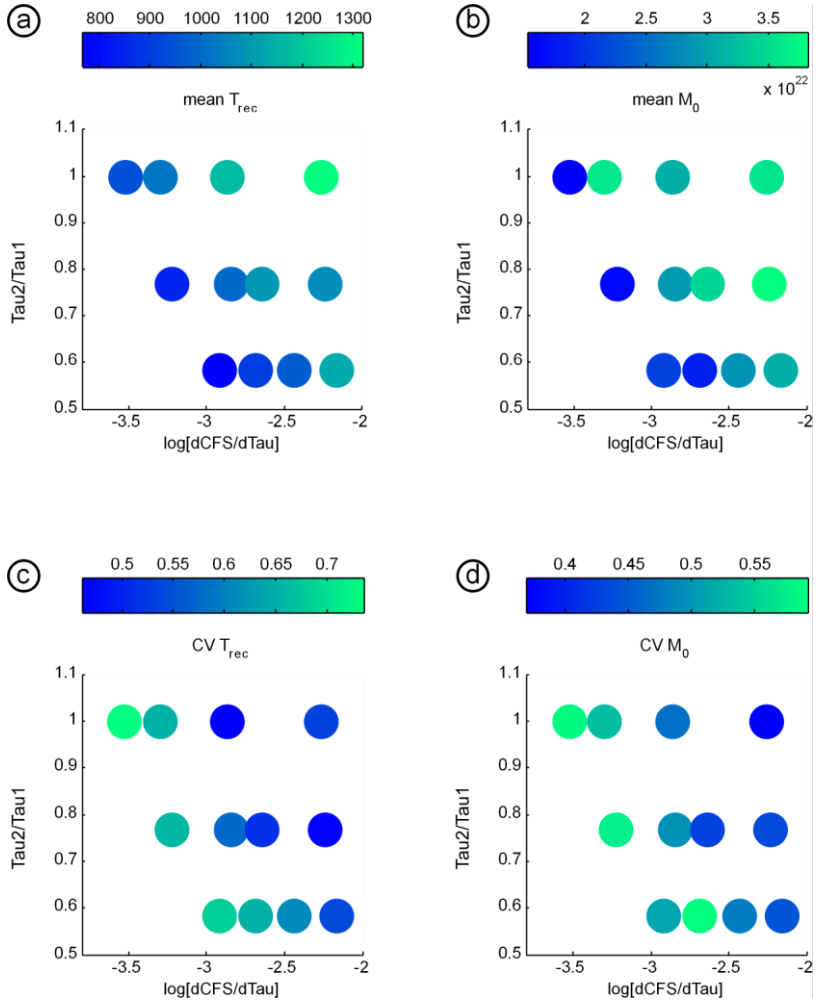

Figure 6: Correlation between of recurrence time (a, c) and seismic moment (b, d) with stress coupling (dCFS/dTau) and strength contrast (Tau2/Tau1). See table A1 for regression analysis results.

The significant trends of M_0 and T_{rec} with dCFS/dTau are replotted in Figure 7 with a differentiation between all events (solo and double events) and solo events to explore the effects of stress coupling on the frequency-size distributions in more detail. Consistently, considering only double events increases mean seismic moment and mean recurrence time and decreases the associated CVs. This is simply a result of setting a magnitude threshold.

More interestingly, however, is the observation that the trends differ for the two groups of events: For example, the positive correlation of Trec with stress coupling observed for all events is inverted to a negative correlation if only double events are considered (Fig. 7a). This is simply the result of double events being systematically rarer in more weakly coupled

systems as has been predicted by Ruff (1996). At the same time, recurrence times of double events are more sensitive to stress coupling than the recurrence times of all events: Double events recur almost randomly for weakly coupled systems and periodically for strongly coupled systems as suggested by a CV of T_{rec} ranging between 1 and 0.1. On the other side, the CV of M_0 is much smaller (0.2) and independent of stress coupling indicating a characteristic size of double events.

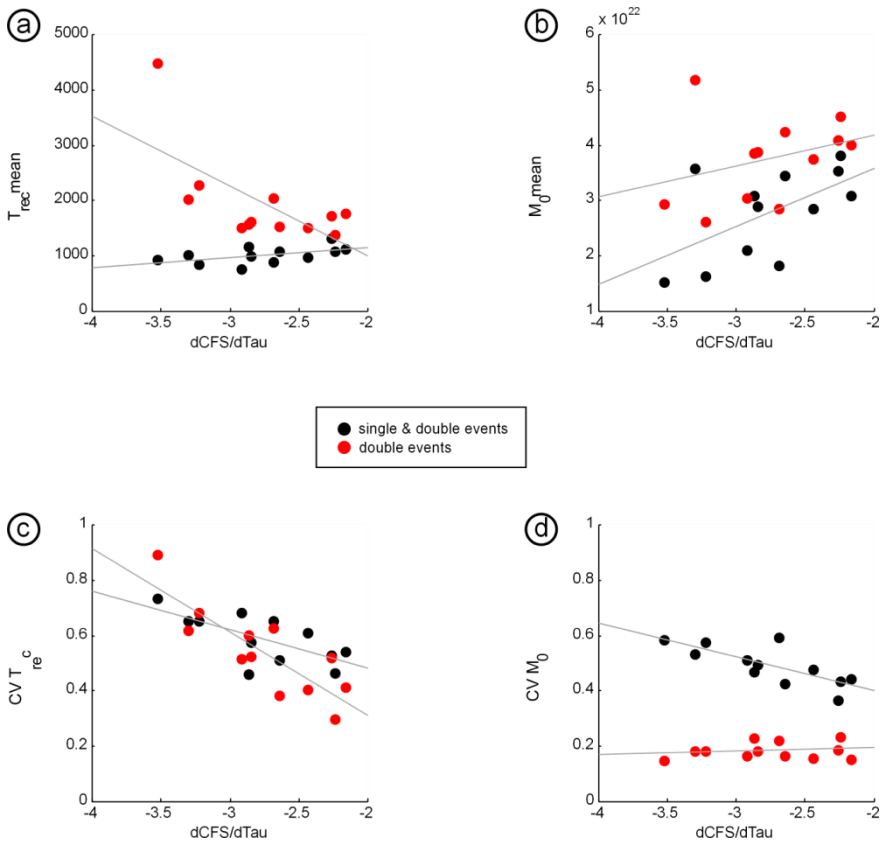

Figure 7: Correlation between of recurrence time (a) and its CV (c) and seismic moment (b) its CV (d) with stress coupling (dCFS/dTau) for all events (black dots) and double events (red dots).

4 Discussion: Proxies for barrier efficiency

We simulated long time-series of analog subduction megathrust earthquakes in order to constrain the recurrence pattern of a simple system with two asperities coupled by static stress transfer. Similar experiments (Corbi et al. 2017) and numerical simulations (Kaneko et al

2010) have been carried out to find the critical parameters controlling the probability of a rupture bridging the barrier and causing a synchronized failure of the asperities. We here add experimental data representing a different set of material parameters and geometries which allows testing the existing concepts and to identify the minimum set of parameters needed.

Kaneko et al. (2010) suggested a set of parameters combined in a proxy for barrier efficiency called B. B is the ratio of the stress increase required to bridge the barrier to the coseismic stress drop. B included parameters which are directly and indirectly (involving assumptions) observable in nature (geometric, kinematic, dynamic and friction parameters). Given the complexity of B and the uncertainty in the choice of some of the parameters included (e.g. frictional parameters), Corbi et al. (2017) aimed at a more simple proxy based solely on first-order geometric relationships easy to observe in nature, i.e. the barrier-to-asperity length ratio Db/Da. With respect to these two proxies, we consider the stress coupling as defined here as a proxy for barrier efficiency of intermediate complexity. Similar to Db/Da, stress coupling can be inferred primarily from geometric observations (size and location of asperities).

In Figure 8 we compare the three proxies based on the setup presented in this study. Obviously, there is a good correlation between stress coupling, B and Db/Da. Db/Da seems slightly more sensitive to stress coupling than B as suggested by its steeper slope. In any case, a correlation coefficient (R^2) of 0.6 to 0.8 suggests general interoperability of the three proxies.

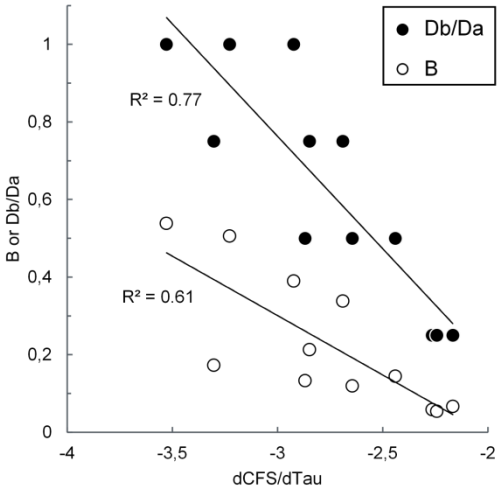

406

407 **Figure 8:** Correlation of stress coupling stress coupling with B and Db/Da parameters.

408 Figure 9 shows the collapse of all existing experimental, numerical and real world data in a
409 plot of percentage synchronized ruptures (double events) versus B while plotting those data
410 against Db/Da separates the data into roughly parallel trends. Because the data used represent
411 a wide spectrum of geometrical and rheological parameters, the collapse indicates the
412 versatile nature of the proxy B for anticipating double events.

413 On the other hand, the systematic offset trends suggest that while Db/Da seems to allow for a
414 strong control on synchronization, material properties cannot be neglected. For instance, it
415 appears that the setup used in the present study generates double events more easily. While
416 for the experiments by Corbi et al. (2017) and the natural example a threshold for double
417 events at Db/Da of 0.5 emerges, in the experiments presented here this threshold is
418 significantly higher (>1). This suggests that the barrier in the Corbi et al. (2017) experiments
419 as well as in the Nankai area are mechanically more effective than in our setup.

420 We conclude that for the moment, the full complexity of the proxy B by Kaneko et al. (2010)
421 is needed to account for the variability of mechanical parameters present in the experiments.

To which extent these parameters vary in nature and therefore control the threshold value of Db/Da remains to be explored.

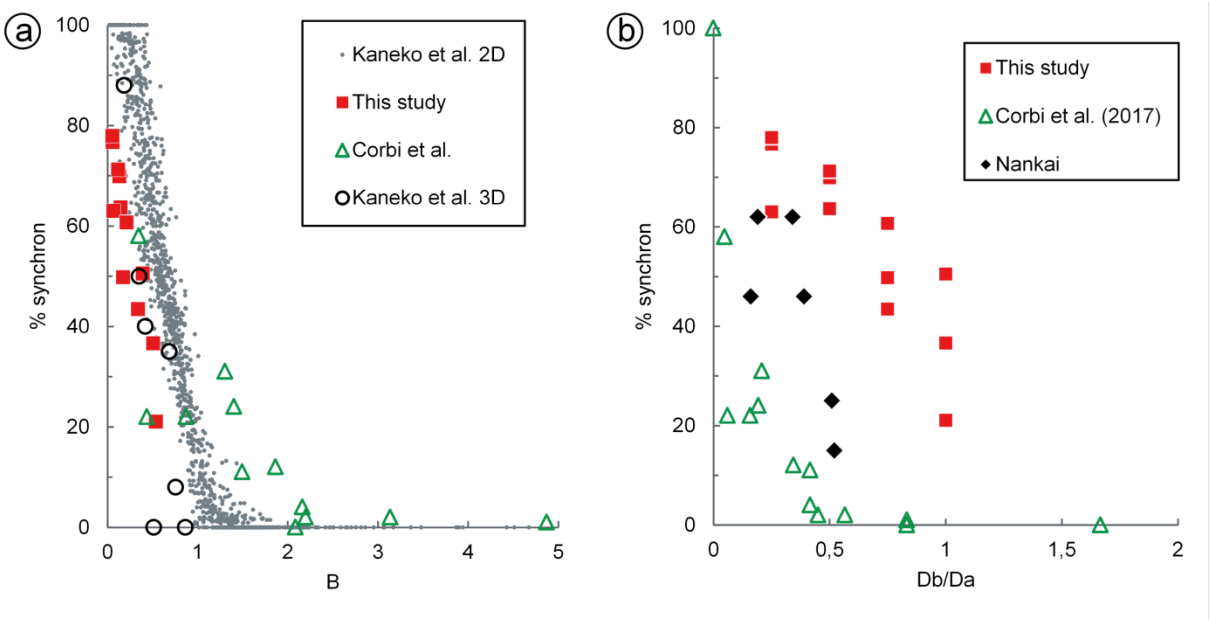

Figure 9: Probability of synchronous events as a function of B (a) and Db/Da (b). Note collapse of experimental, natural and numerical simulation data in (a). Parallel offset trends in (b) are interpreted as due to differences in frictional properties between the experiments and nature.

5 Conclusions

Based on experiments generating long time-series of analog subduction megathrust earthquakes we explored the process of synchronization of two velocity-weakening asperities separated by a velocity-strengthening barrier. We found the following:

- Synchronization is controlled by the static stress transfer from a one asperity to the other, quantified by the stress coupling dCFS/sTau. Accordingly, the percentage of synchronized events scales with the logarithm of (normalized) Coulomb stress change on the receiver asperity.

- A strength contrast between the two asperities has no significant effect on synchronization but decreases the recurrence time of double events because the weaker asperity dictates the recurrence intervals.
- Analogue earthquakes in strongly coupled systems recur more periodically and with a more characteristic size than in weakly coupled systems.

Three proxies for the barrier efficiency, B (Kaneko et al. 2010), Db/Da (Corbi et al., 2017) and the newly defined stress coupling have been cross-validated and tested for applicability:

- Db/Da is the most simple and easiest to apply proxy and incorporates the most sensitive parameters to work first-order. It relies on geometries which – if they are stationary over multiple seismic cycles - we are able to constrain using interseismic locking and paleoseismological observations.
- B is the most versatile proxy and it captures the physics - but several parameters are not well constrained or uncertain in nature.
- Stress coupling is of intermediate complexity and interoperable with Db/Da and B.

In order to arrive at a minimum set of parameters necessary to describe seismic hazard in subduction zones we suggest to further explore the variability of those parameters in B which are not well known in nature, to define the sensitivity of simpler proxies and to aim at constraining their upper and lower bounds.

Acknowledgements

This study has been partially funded by the German Research Foundation (DFG) collaborative research center SFB1114 “Scaling Cascades in Complex Systems”, project B01. FC received funding from the European Union’s Horizon 2020 research and innovation

459 program under the Marie Sklodowska-Curie grant agreement 658034 (AspSync). We thank Y.
460 Kaneko for sharing his data to populate Figure 9a.

461

References

Adam, J., O. Oncken, N. Kukowski, J. Lohrmann, S. Hoth, J. L. Urai, W. van der Zee, J. Schmatz, B. Wieneke, and K. Pfeiffer (2005), Shear localisation and strain distribution during tectonic faulting - New insights from granular-flow experiments and high-resolution optical image correlation techniques, Journal of Structural Geology, 27(2), 183-301, doi:10.1016/j.jsg.2004.08.008.

Caniven, Y., Dominguez, S., Soliva, Roger., Cattin, R., Peyret, M.,Marchandon, M. Romano, C, Strak, V. (2015). A new multilayered visco-elasto-plastic experimental model to study strike-slip fault seismic cycle. Tectonics, 34, 232-264, doi:1002/2014TC003701.

Yannick Caniven, Stéphane Dominguez, Roger Soliva, Michel Peyret, Rodolphe Cattin, Frantz Maerten, (2017), Relationships between along-fault heterogeneous normal stress and fault slip patterns during the seismic cycle: Insights from a strike-slip fault laboratory model, In Earth and Planetary Science Letters, Volume 480, Pages 147-157, ISSN 0012-821X, https://doi.org/10.1016/j.epsl.2017.10.009.

Corbi, F., F. Funiciello, M. Moroni, Y. van Dinther, P. M. Mai, L. A. Dalguer, and C. Faccenna (2013), The seismic cycle at subduction thrusts: 1. Insights from laboratory models, J. Geophys. Res. Solid Earth, 118, 1483–1501, doi:10.1029/2012JB009481.

Corbi, F., F. Funiciello, S. Brizzi, S. Lallemand, and M. C. G. L. Rosenau (2017): Control of asperities size and spacing on seismic behavior of subduction megathrusts, Geopys. Res. Letters, 44,

Franzke, C., O'Kane, T., Monselesan, D., Risbey, J. and Horenko,I. (2015), Systematic Attribution of Secular Southern Hemispheric Circulation Trends with Observational Forcing Data, Nonlin. Proc. Geophys., 22: 513-525.

485 Horenko, I. (2009), On robust estimation of low-frequency variability trends in discrete
486 Markovian sequences of atmospheric circulation patterns. J. of Atmos. Sci., 66(11):1941-
487 1954.

488 Horenko, I. (2010), Finite element approach to clustering of multidimensional time series.
489 SIAM J. of Sci. Comp., 32(1):62-83.

490 Hubbert, M. K. (1937), Theory of scale models as applied to the study of geological
491 structures, Geological Society America Bulletin, 48, 459-1520.

492 Kaiser, O. Igdalov, D. and Horenko, I. (2015), "Statistical regression analysis of threshold
493 excesses with systematically missing covariates." SIAM Multiscale Modeling & Simulation
494 (SIAM MMS) , 13(2):594-613.

495 O'Kane, T. , Risbey, J. ,Monselesan, D., Horenko, I. and Franzke, C. (2016), "On the
496 dynamics of persistent states and their secular trends in the waveguides of the southern
497 hemisphere troposphere." Climate Dynamics , 46(11-12):3567-3597.

498 Risbey, J., O'Kane, T., Monselesan, D, Franzke, C. and Horenko, I. (2015), "Metastability of
499 Northern Hemisphere teleconnection modes." J. Atmos. Sci., 72:35-54.

500 Kaneko, Y., J. P. Avouac, and N. Lapusta (2010), Towards inferring earthquake patterns from
501 geodetic observations of interseismic coupling, Nature Geoscience, 3(5), 363-U324,
502 doi:10.1038/ngeo843.

503 King, G. C. P., R. S. Stein, and J. Lin (1994), Static stress changes and the triggering of
504 earthquakes, Bulletin of the Seismological Society of America, 84(3), 935-953.

505 Kuehn, N. M., S. Hainzl, and F. Scherbaum (2008), Non-Poissonian earthquake occurrence in
506 coupled stress release models and its effect on seismic hazard, Geophys. J. Int., 174, 649–658,
507 doi:10.1111/j.1365-246X.2008.03835.x.

547 Lin, J., Stein, R.S. (2004), Stress triggering in thrust and subduction earthquakes and stress
548 interaction between the southern San Andreas and nearby thrust and strike-slip faults, Journal
549 of Geophysical Research, 109, doi:10.1029/2003JB002607.

550 Metzner, P Putzig, L. and Horenko, I. (2012) "Analysis of persistent non-stationary time
551 series and applications." Comm. in Appl. Math. and Comp. Sci. (CAMCoS), 7(2):175-229.

552 Okada, Y. (1985), Surface deformation due to shear and tensile faults in a half-space, Bulletin
553 of the Seismological Society of America, 75(4), 1135-1154.

554 Okada, Y. (1992), Internal deformation due to shear and tensile faults in a half-space, Bulletin
555 of the Seismological Society of America, 82(2), 1018-1040.

556 Rosenau, M., F. Corbi, and S. Dominguez (2017), Analogue earthquakes and seismic cycles:
557 Experimental modelling across timescales, Solid Earth, 8, 3, 1-65, doi.: 10.5194/se-8-597-
558 2017

559 Rosenau, M., J. Lohrmann, and O. Oncken (2009), Shocks in a box: An analogue model of
560 subduction earthquake cycles with application to seismotectonic forearc evolution, Journal of
561 Geophysical Research-Solid Earth, 114, 20, doi: 10.1029/2008jb005665.

562 Rosenau, M., R. Nerlich, S. Brune, and O. Oncken (2010), Experimental insights into the
563 scaling and variability of local tsunamis triggered by giant subduction megathrust
564 earthquakes, Journal of Geophysical Research-Solid Earth, 115, doi:10.1029/2009jb007100.

565 Rosenau, M., and O. Oncken (2009), Fore-arc deformation controls frequency-size
566 distribution of megathrust earthquakes in subduction zones, Journal of Geophysical Research-
567 Solid Earth, 114, 12, doi:10.1029/2009jb006359.

568 Ruff, L. J. (1996), Large Earthquakes in Subduction Zones: Segment Interaction and
569 Recurrence Times, in Subduction Top to Bottom, edited, pp. 91-104, American Geophysical
570 Union.

571 Scholz, C. H. (1998), Earthquakes and friction laws, Nature, 391, 37-42.

572 Shearer, P.M., Stark, P.B. (2012), Global risk of big earthquakes has not recently increased,
573 Proceedings of the National Academy of Sciences of the United States of America, 109 (3),
574 pp. 717-721. DOI: 10.1073/pnas.1118525109

575 Shreve, R. L., and Cloos, M. (1986), Dynamics of sediment subduction, melange formation,
576 and prism accretion, Journal of Geophysical Research, 91, 10229 –10245.

577 Toda, S., Stein, R. S. (2002), Response of the San Andreas fault to the 1983 Coalinga-Nuñez
578 Earthquakes: An application of interaction-based probabilities for Parkfield, Journal of
579 Geophysical Research, 107, doi:0.1029/2001JB000172.

580 Vercauteren, N., Klein, R. (2015). A clustering method to characterize intermittent bursts of
581 turbulence and interaction with submeso motions in the stable boundary layer. J. Atmos. Sci.,
582 72, 1504-1517
583

584 Tab. A1

585

Parameter *X*	**Parameter *Y***	***R²***
dCFS/DTau	T_{rec}	0.285
dCFS/DTau	M_0	0.333
dCFS/DTau	*CV* T_{rec}	0.475
dCFS/DTau	*CV* M_0	0.588
Tau1/Tau2	T_{rec}	0.245
Tau1/Tau2	M_0	0.055
Tau1/Tau2	*CV* T_{rec}	0.012
Tau1/Tau2	*CV* M_0	0.010

586
587 **Table A1:** Results from linear regression analysis (green = statistically significant; red = insignificant).See

588 Figure 6 for visulalization of trends.

Fig. A1

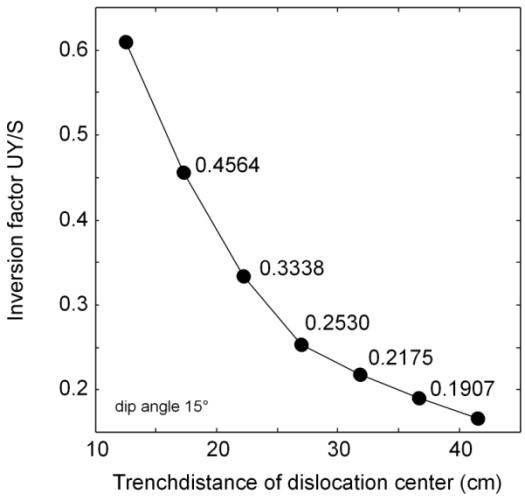

589

590 **Figure A1:** Relation between horizontal surface displacement and slip on dislocation as a function of trench

591 distance (depth).

Fig.A2

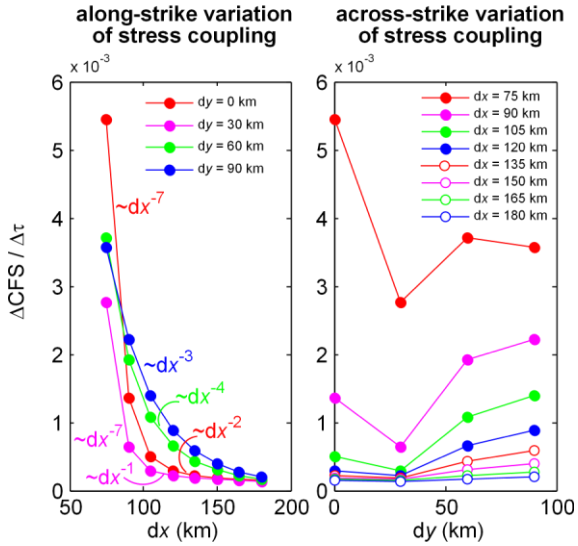

592

593 **Figure A2:** Spatial variation of coulomb stress transfer along strike and across strike of the subduction zone as

594 predicted by elastic dislocation modelling. Definition of dx and dy see main text.

Fig. A3

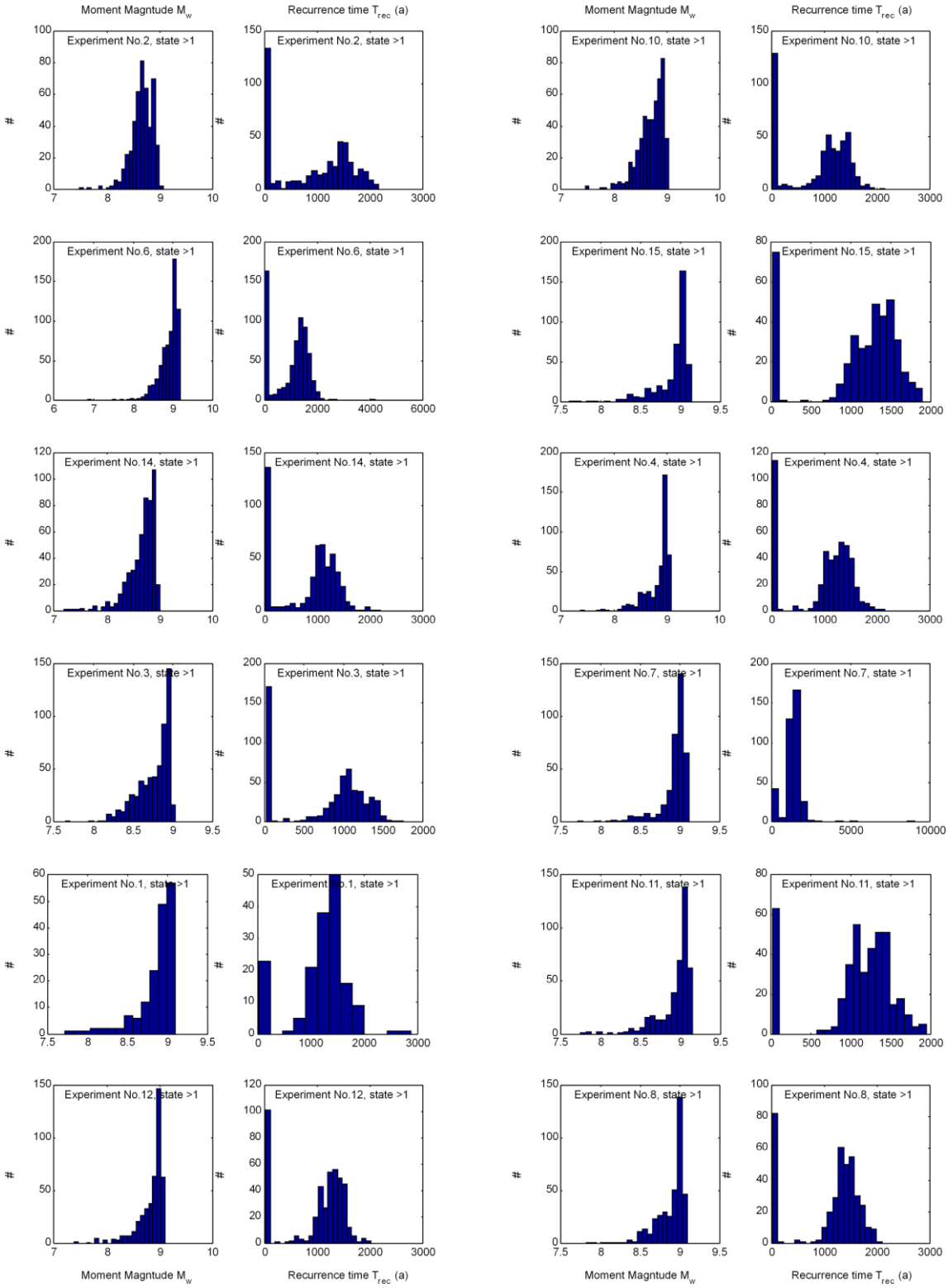

595

596 **Figure A3:** Probability distribution functions (pdfs) of Mw and Trec for all experiments. The order of the plots

597 is such that in the two rows experiments increase in stress coupling downwards. Second row is continuation of

598 first row.